

# **Steady Viscous Flow in a Triangular Cavity**

**Calvin J. Ribbens, Layne T. Watson,  
and C.-Y. Wang**

**TR 92-21**

Department of Computer Science  
Virginia Polytechnic Institute and State University  
Blacksburg, Virginia 24061

May 8, 1992

# STEADY VISCOUS FLOW IN A TRIANGULAR CAVITY

CALVIN J. RIBBENS,<sup>1</sup> LAYNE T. WATSON<sup>1</sup> and C.-Y. WANG<sup>2</sup>

<sup>1</sup>Department of Computer Science, Virginia Polytechnic Institute & State University, Blacksburg, VA 24061, U.S.A.

<sup>2</sup>Departments of Mathematics and Mechanical Engineering, Michigan State University, East Lansing, MI 48824, U.S.A.

**Abstract**—Steady recirculating viscous flow inside an equilateral triangular cavity is generated by translating one side. The Navier-Stokes equations are solved numerically using finite differences on a transformed geometry. The results show a primary eddy and a series of secondary eddies at the stagnant corner. For high Reynolds numbers the interior of the primary eddy has constant vorticity, but its value can not be predicted by the mean-squared law.

## 1. INTRODUCTION

Steady recirculating flow is a basic phenomenon in fluid mechanics. Such flows occur in the near wake of moving bluff bodies, in channel flows with abrupt constrictions, or inside cavities partially bounded by solid surfaces. The most studied case in the literature is the cavity flow, a viscous fluid enclosed by solid boundaries except for a translating segment which drives the recirculation through shear stress. This type of flow is important not only in its own right as a basic physical model, but due to its simple geometry, also serves as a test problem for numerical algorithms.

Not surprisingly, the most widely used geometry for recirculating cavity flow in the literature is a two dimensional square enclosure with one side translating with uniform velocity. Experimental observations of the streamlines were recorded by Mills [1] and Pan and Acrivos [2] for Reynolds number, defined as (translation velocity) · width/(kinematic viscosity), up to order of 1000. Due to the extreme nonlinearity of the Navier-Stokes equations, little analytic work can be done. In the limit of infinite Reynolds number, Batchelor [3] predicted analytically that the interior would attain constant vorticity given by a mean squared law. A variety of methods are used to solve the problem numerically—finite differences, false transients, multi-grid methods, etc. (e.g., Burggraf [4], Tuann and Olson [5], Ghia et al. [6], Schreiber and Keller [7]). It is generally agreed that there is a dominant recirculation whose center is closer to the moving wall. As the Reynolds number is increased, this center first moves downstream, then moves towards the middle of the square. There are two small counter recirculating eddies at the stagnant corners. The vorticity is most intense near the moving boundary. For high Reynolds numbers the vorticity is confined to a boundary layer and the interior vorticity is approximately constant.

However, there are also some differences in the numerical results. The existence of a third small counter rotating eddy upstream of the moving plate has not been accepted by all numerical researchers, nor was it observed experimentally. The numerical scheme of Benjamin and Denny [8] showed enlargement of the small eddies as the Reynolds number is increased, opposite to the conclusion of others. There is also extreme difficulty in increasing the Reynolds number to the extent that Batchelor's theoretical mean-square law [3] can be convincingly confirmed. Finally Schreiber and Keller [9] showed that a computational mesh not sufficiently small would lead to spurious solutions, implicating many earlier numerical calculations may be erroneous.

Instead of proposing yet another method to treat the square cavity problem, the present paper studies numerically the triangular cavity, which has not been done before. A triangular groove is more common than a square groove on surfaces which have been roughened by scoring. Our aim

is to determine the structure of the recirculating flow and the numerical difficulties peculiar to the triangular geometry.

## 2. FORMULATION

Let  $\Omega$  be the equilateral triangle with corners  $(-\sqrt{3}a, a)$ ,  $(\sqrt{3}a, a)$ , and  $(0, -2a)$ , and let  $\partial\Omega$  be the boundary of  $\Omega$ . The two-dimensional steady Navier-Stokes equations are

$$u' u'_{x'} + v' u'_{y'} = -\frac{1}{\rho} p'_{x'} + \nu (u'_{x'x'} + u'_{y'y'}), \quad (1)$$

$$u' v'_{x'} + v' v'_{y'} = -\frac{1}{\rho} p'_{y'} + \nu (v'_{x'x'} + v'_{y'y'}), \quad (2)$$

$$u'_{x'} + v'_{y'} = 0. \quad (3)$$

Here  $u'$ ,  $v'$  are velocity components in the Cartesian  $x'$ ,  $y'$  directions,  $\rho$  is the density,  $p'$  is the pressure, and  $\nu$  is the kinematic viscosity. The boundary conditions are no slip on sides of the triangle moving with a velocity of constant magnitude  $U$ , on fixed sides the velocity is zero, and velocities are bounded inside  $\Omega$ . We normalize all velocities by  $U$ , the pressure by  $\rho U^2$ , the lengths by  $a$ , and drop primes. Define a stream function  $\psi$  by

$$u = \psi_y, \quad v = -\psi_x. \quad (4)$$

The governing equations in  $\Omega$  become

$$\nabla^4 \psi = R (\psi_y \nabla^2 \psi_x - \psi_x \nabla^2 \psi_y), \quad (5)$$

where  $\nabla^2$  is the Laplacian operator and  $R$  is the Reynolds number  $Ua/\nu$ . The boundary conditions become

$$\psi = 0 \text{ on all three sides of } \Omega, \quad (6)$$

and

$$(\psi_y, -\psi_x) \cdot \mathbf{T} = \begin{cases} 1, & \text{for the top side,} \\ 0, & \text{for the other two sides,} \end{cases} \quad (7)$$

where  $\mathbf{T}$  is a unit vector tangent to the boundary pointing in the direction of motion (clockwise). Equation (7) determines the magnitude of the velocity vector  $(\psi_y, -\psi_x)$ . The direction of the velocity is already determined (up to sign) by (6), since  $\psi = 0$  on  $\partial\Omega$  implies  $\nabla\psi = (\psi_x, \psi_y)$  is normal to a side; and thus the velocity, which is normal to  $\nabla\psi$ , must be tangent to the boundary. For the equilateral triangle  $\Omega$  considered here, equation (6) can be written

$$\begin{aligned} \psi_y &= 1, \text{ on the top side,} \\ \sqrt{3}\psi_x - \psi_y &= 0, \text{ on the right side,} \\ \sqrt{3}\psi_x + \psi_y &= 0, \text{ on the left side.} \end{aligned} \quad (8)$$

## 3. NUMERICAL METHODS

We apply a Newton-like iteration to equation (5). It is well known that if Newton's method converges to the root of a nonlinear equation, it does so rapidly. However, a good initial guess

is usually needed for convergence to occur. We use a very simple initial guess, namely a cubic polynomial constructed to be zero on  $\partial\Omega$ . For the equilateral triangle we choose

$$\psi^{(0)}(x, y) = -(y - 1)(\sqrt{3}x + y + 2)(\sqrt{3}x - y - 2), \quad (9)$$

while for the right triangle discussed in Section 3.1 below we use

$$\psi^{(0)}(x, y) = xy(x + y - 2\sqrt{3}). \quad (10)$$

Rapid convergence is achieved for  $R = 1$  in all cases with sufficiently fine grids. Solutions for higher Reynolds number in a given case are computed by using as initial guess a solution for a slightly smaller  $R$  for the same case.

A Newton-like linearization of the nonlinear operator in Equation (5) results in the following linear fourth order PDE to be solved at each iteration:

$$\nabla^4 \psi - R \left( \psi_y^{(i)} \nabla^2 \psi_x + \nabla^2 \psi_x^{(i)} \psi_y - \psi_x^{(i)} \nabla^2 \psi_y - \nabla^2 \psi_y^{(i)} \psi_x \right) = -R \left( \psi_y^{(i)} \nabla^2 \psi_x^{(i)} - \psi_x^{(i)} \nabla^2 \psi_y^{(i)} \right), \quad (11)$$

where  $\psi^{(i)}$  is the approximate solution from the previous step. See Ribbens et al. [10] for a more detailed derivation of (11). At each step of the outer iteration we must solve the linear problem defined by Equations (6), (8), and (11). Notice that linearization precedes discretization. One could also discretize first and then deal with the resulting system of nonlinear equations, but the two approaches are essentially equivalent.

### 3.1 Finite differences on original problem

An efficient numerical technique for solving the related driven cavity problem is described by Schreiber and Keller [7]. The classical driven cavity problem describes steady viscous incompressible flow in the unit square, with one side moving. The technique employed in [7] is based on central differences and a uniform rectangular grid, yielding a discretization with second order accuracy. The difference formulas used to approximate the derivative terms in both the PDE and the boundary conditions are centered. A 13 point stencil is required for the fourth-order derivatives. In order to impose the PDE at grid points just inside the region, “fictional” grid points just exterior to the boundary are required, but the unknown  $\psi$  values at these exterior grid points are determined by imposing the normal derivative boundary condition at nearby boundary grid points. The technique in [7] also includes continuation in the Reynolds number, a special sparse direct factorization scheme for the resulting linear systems, and Richardson extrapolation for improved accuracy.

We considered modifying the approach of Schreiber and Keller for the triangle problem. Unfortunately, the equilateral triangle presents considerable difficulties under such an approach. Figure 1 shows a typical case. As in Ref. [7], we introduce grid points just external to the region. Each external point above the top edge is eliminated by hand by imposing the derivative boundary condition (8) at the boundary grid point directly beneath it. The unknown value at an external grid point along the left or right side is determined by imposing the derivative boundary condition at the boundary grid point immediately above that point. Centered formulas are used for the derivatives in these boundary conditions for all but two points. Notice that no external points are defined just above or below the upper left and right corners. The reason is that introducing such points would immediately lead to a singular system, since there is only one nearby boundary point (the corner itself) at which to enforce boundary conditions, but we would have two new fictional

- symmetric boundary formulas
- ⊗ one-sided boundary formulas
- ⊕ PDE -- symmetric formulas
- ⊖ PDE -- unsymmetric formulas
- function values only

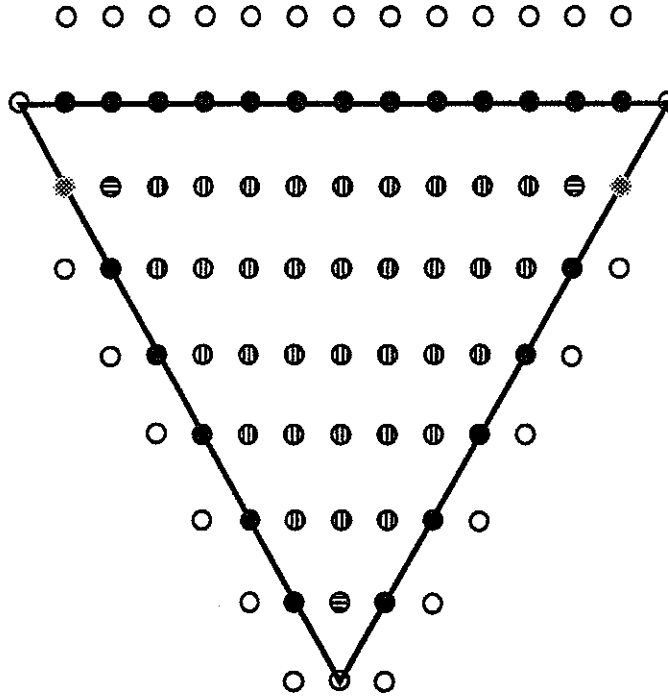


Fig. 1. Equations and unknowns for the equilateral triangle  $\Omega$ .

points. Furthermore, the derivative boundary conditions are not well defined at the corners, so imposing them in an arbitrary direction seems dangerous. Similarly, we do not have an external grid point beneath the bottom corner because the derivative boundary condition is not defined at the corner. The immediate result of this special treatment near the corners is that we must use nonsymmetric stencils for the  $x$  derivatives at the boundary grid points nearest the two upper corners, and we must use nonsymmetric 18 point stencils for the PDE at the interior points nearest all three corners. For the remaining interior grid points the standard 13 point finite difference stencil suffices.

Despite our relatively straightforward generalization of the technique of Schreiber and Keller, the linear systems generated by the method just described are so ill conditioned that accurate numerical solutions are virtually impossible. In fact, for moderately fine grids (e.g., 49 vertical grid lines and 25 horizontal grid lines) the systems are numerically singular, with condition numbers in excess of  $10^{13}$ . The problem is related to the special treatment required in the corners and to the overlapping stencils needed for the derivative boundary equations along the left and right sides. On a test problem, if we assume the external solution values are known, so that neither the

one-sided stencils nor the derivative boundary equations are needed, the linear systems become quite well conditioned (e.g.,  $10^3$  for the case mentioned above). We did not pursue further the causes of the ill conditioning or seek remedies, as the approach described in the next section proved successful. However, it is interesting to note the significant problems that arise in modifying the straightforward difference method of Schreiber and Keller for the triangle.

### 3.2 Other approaches

In a previous paper [10] we described a numerical technique for solving the related problem of flow induced in an elliptic region by the boundary moving at constant velocity. In that work our numerical approach was based on collocation with Hermite cubic basis functions, and we defined the problem as a coupled system of two second order equations in two unknowns (stream function and vorticity). This strategy proved quite successful and yielded accurate solutions for Reynolds number up to 1000 and for ellipses with aspect ratio up to 5.

An analogous strategy for the present problem is not successful, however. As in the finite difference method described above, special problems near the corners lead to nearly singular linear systems, and in fact to exactly singular systems if the collocation points are not chosen carefully. Our experience is that this extreme ill conditioning causes inaccuracies in the approximate solution, and prevents the Newton iteration from converging for all but the smallest Reynolds numbers. Neither collocation nor centered finite differences applied to the system of two second order equations was successful.

### 3.3. Finite differences on transformed problem

Returning to a direct finite difference treatment of the fourth order problem, a more successful numerical treatment is possible. The key step is to transform the problem to an equivalent problem posed on a right triangle. In particular, we introduced a change of variables

$$\xi = x + (y + 2)/\sqrt{3} \text{ and } \eta = 2(1 - y)/\sqrt{3},$$

so that our computational region is a right triangle  $\tilde{\Omega}$  with corners  $(0, 0)$ ,  $(2\sqrt{3}, 0)$ , and  $(0, 2\sqrt{3})$ . The transformed PDE operator in  $\xi, \eta$  is a very general one indeed, since the chain rule produces terms of up to total (derivative) degree 4 with coefficients depending on the coefficients of the original problem and on the transformation. Deriving the transformed coefficients and new difference formulas for all of these derivative terms by hand would be extremely tedious. We found the process reasonably straightforward, however, using the symbolic computational facilities of Mathematica [11].

The most important benefit of transforming the problem to a right triangle is that the transformed derivative boundary conditions are still simply normal derivative conditions on  $\tilde{\psi}$ , the unknown in  $\tilde{\Omega}$  (i.e., a Neumann condition). This is precisely true only for an equilateral triangle transformed to an isosceles right triangle. The original problem posed on a scalene triangle might be unavoidably ill conditioned—this remains a topic for future work. This Neumann boundary condition is extremely important for the numerical scheme because it allows us to use centered difference formulas to approximate these derivative conditions, and because these formulas do not overlap (as they do on the equilateral triangle). As can be seen in Fig. 2, we again introduce unknowns exterior to the region and eliminate them by hand by imposing the derivative boundary condition at the nearest point on the boundary. Note that along the hypotenuse of the triangle we impose the derivative boundary condition at the midpoint of a grid square rather than on a

- symmetric boundary formulas
- ⊕ PDE
- function values only

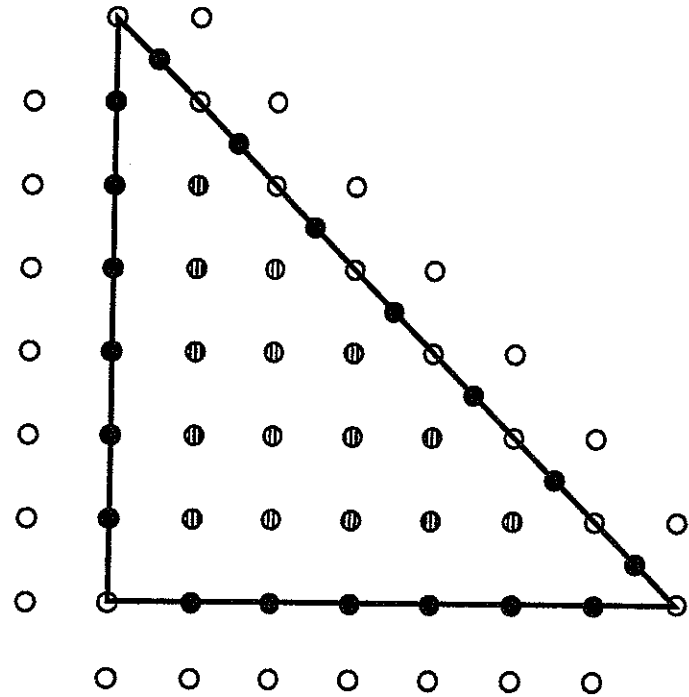


Fig. 2. Equations and unknowns for the right triangle  $\tilde{\Omega}$ .

grid point. There are several possibilities for second order accurate finite difference stencils in the interior of the region. As can be seen in Fig. 3, the stencil we use is skewed so that it "fits" the geometry. Thus, we are able to use the same difference equations to approximate the PDE at all interior points, including those closest to the corners. This is another important benefit of the transformed problem approach. Figure 3 shows the stencil for the PDE applied at the interior grid point closest to the top corner. Other second order accurate stencils require an extra diagonal of fictional points along the hypotenuse. The coefficients for the various finite difference approximations based on this skewed stencil are given in the Appendix.

#### 4. RESULTS

Figure 4 shows the streamline patterns as the Reynolds number is increased. The top boundary is translating to the right, driving the recirculation eddy through viscous shear. For  $R < 1$  the streamlines are almost symmetric with respect to the  $y$  axis. The clockwise primary eddy is about  $4/5$  from the bottom vertex and moves downstream (to the right) as  $R$  is increased. There are several secondary eddies alternating in sign and rapidly decreasing in strength towards the stagnant corner. According to Moffatt's analysis, the size ratio of the eddies for a  $60^\circ$  stagnant corner is about 4.8, which is consistent with our results.

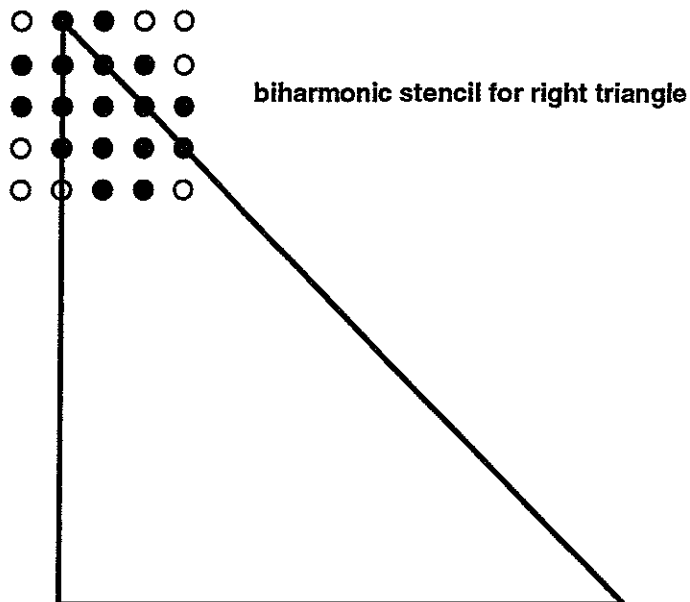


Fig. 3. Stencil for approximating derivatives of up to degree 4 on the right triangle  $\tilde{\Omega}$ . The difference equations for the center point involve unknowns at each of the solid circles.

Figure 5 shows the corresponding vorticity distribution, defined as  $\zeta = \Delta^2 \psi$ . In general vorticity is large and positive near the top, and at large Reynolds numbers, is convected to the right side. Finally at  $R = 500$ , the vorticity changes become more restricted to the boundaries. Figure 6 shows the vorticity distributions for  $R = 500$  along two different directions across the cavity. It is seen that the “interior” of the primary eddy has almost constant vorticity. We define the center  $(x_c, y_c)$  of the primary eddy as the location of maximum  $\psi$  value in the cavity. Table 1 shows that as  $R$  increases to 500, the location of the center  $(x_c, y_c)$ , its stream function value  $\psi_c$ , and its vorticity  $\zeta_c$  all seem to have converged. Similar to the case of the square, the primary eddy center first moves toward the right side, then towards the center of the triangle. Now the fact that  $R = 500$  does not seem to be large is due to our definition of  $R$ . If a side of the triangular cavity is used as the length scale, the actual Reynolds number would be  $2\sqrt{3}$  fold, so our  $R = 500$  is equivalent to a conventional Reynolds number of 1732.

## 5. DISCUSSION AND CONCLUSIONS

Physically the flow in a triangular cavity is similar to the flow in a square cavity. There is, however, only a single stagnant corner where we find a series of small eddies. This phenomena is also shown experimentally for a triangular cavity with a small opening angle (Van Dyke [12]).

Now let us compute the interior constant vorticity predicted by Batchelor [3]. The analytic solution for inviscid rotational flow with constant vorticity inside an equilateral triangle is given by equation (9). Using the mean-square law on the boundary velocity we find the interior vorticity for large  $R$  is  $\sqrt{10}/3 = 1.054$ . This is much lower than our numerical value of 1.250. We conclude Batchelor’s theory does not apply to the triangular cavity. There are several reasons. First, the mean-square law assumes zero pressure gradient along the boundary. The inviscid flow of equation (9), however, shows that pressure rises at the three stagnant corners. Secondly, the assumption of a thin boundary layer enclosing the primary eddy is violated for the triangle. Figure 5e shows secondary eddies occupying large areas. As Figs. 5a–5e show, these secondary eddies seem to get



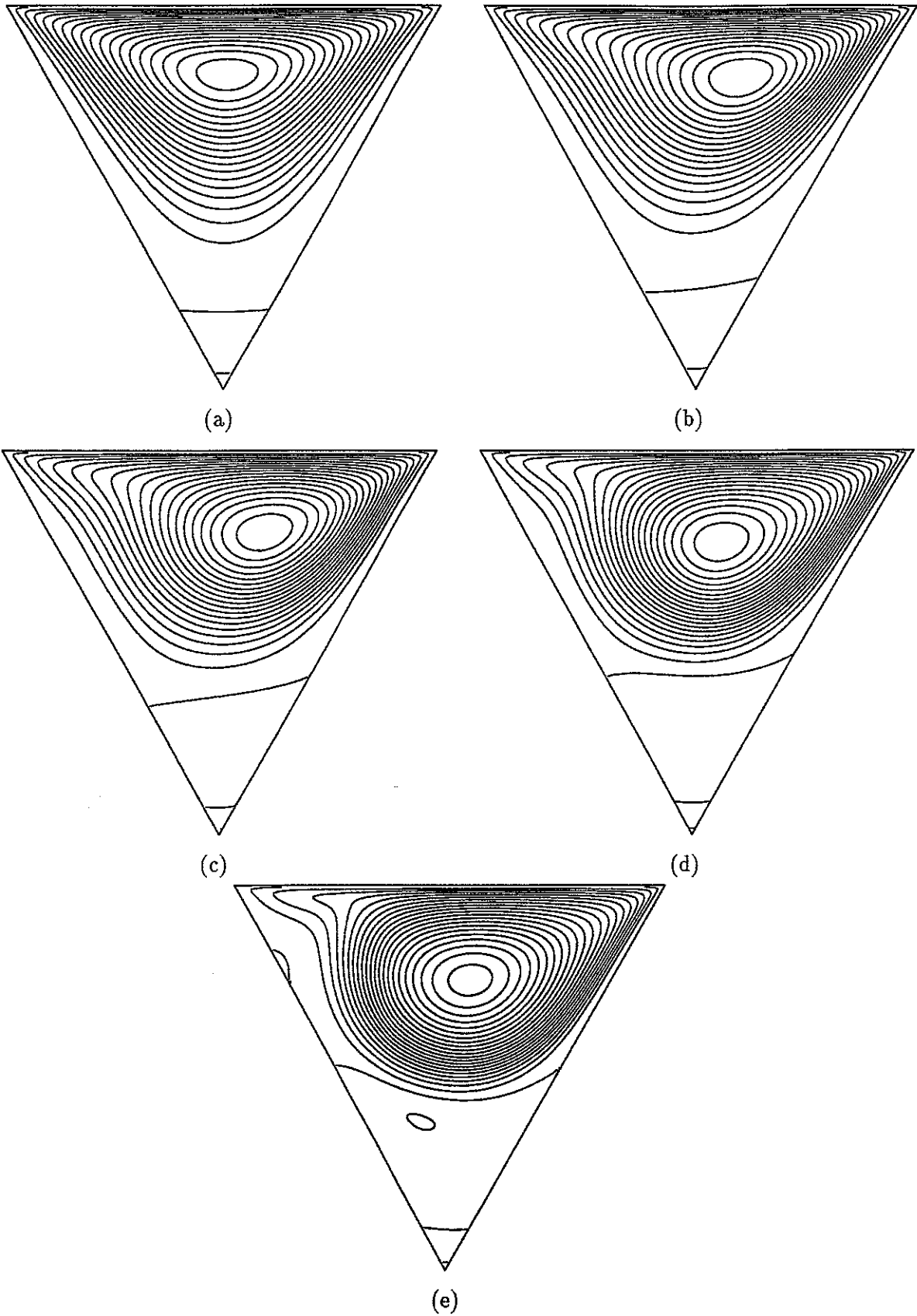


Fig. 4. Streamline patterns for  $R = 1$  (a),  $R = 50$  (b),  $R = 100$  (c),  $R = 200$  (d), and  $R = 500$  (e).

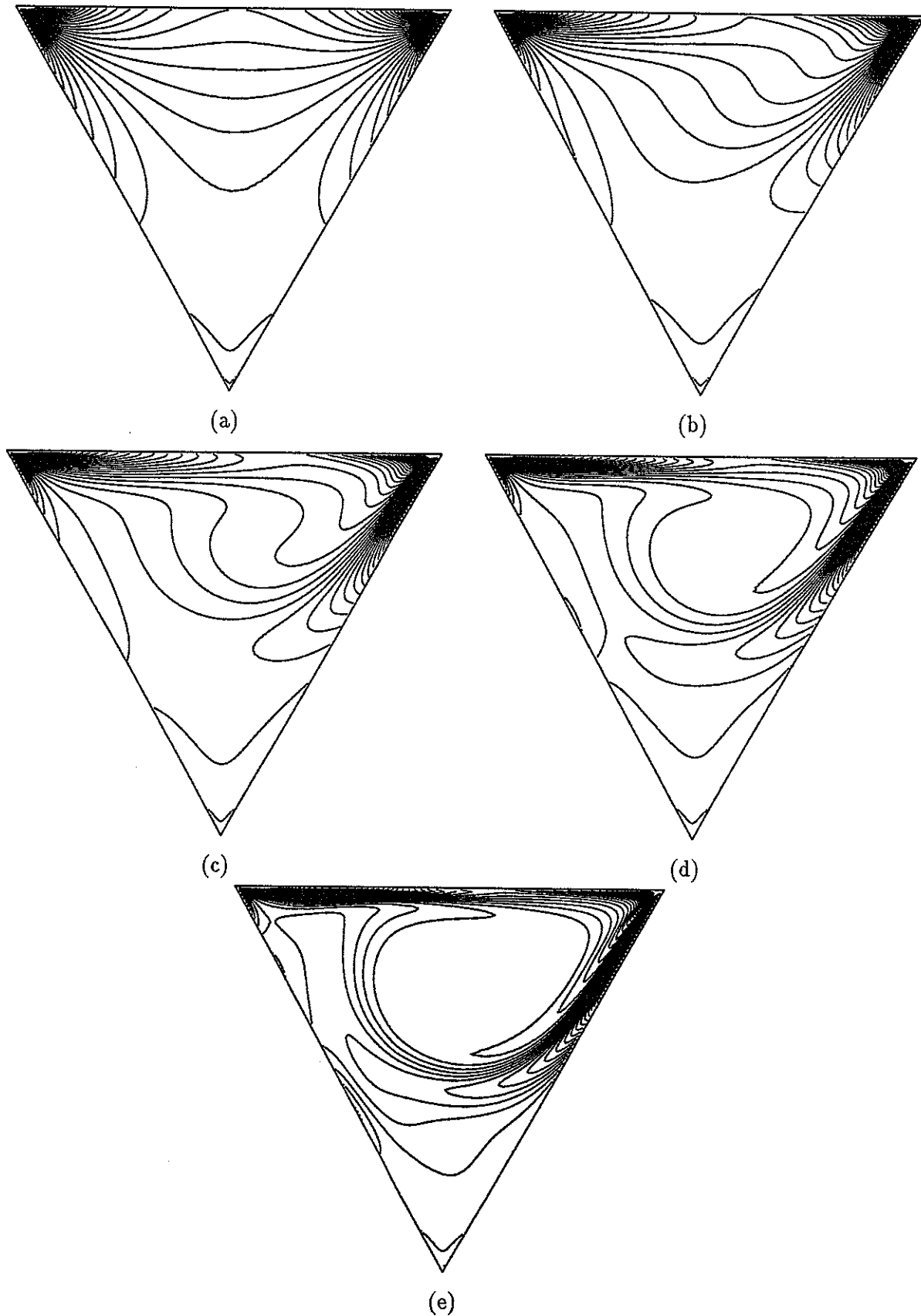


Fig. 5. Vorticity distribution for  $R = 1$  (a),  $R = 50$  (b),  $R = 100$  (c),  $R = 200$  (d), and  $R = 500$  (e).

Table 1. Properties of the center of the primary eddy, located at  $(x_c, y_c)$  with streamfunction value  $\psi_c$  and vorticity  $\zeta_c$ .

$R$	$x_c$	$y_c$	$\psi_c$	$\zeta_c$
1	0.0169	.460	.233	1.363
50	0.346	.445	.237	1.464
100	0.329	.355	.247	1.373
200	0.208	.280	.260	1.272
350	0.173	.265	.268	1.232
500	0.173	.265	.269	1.250

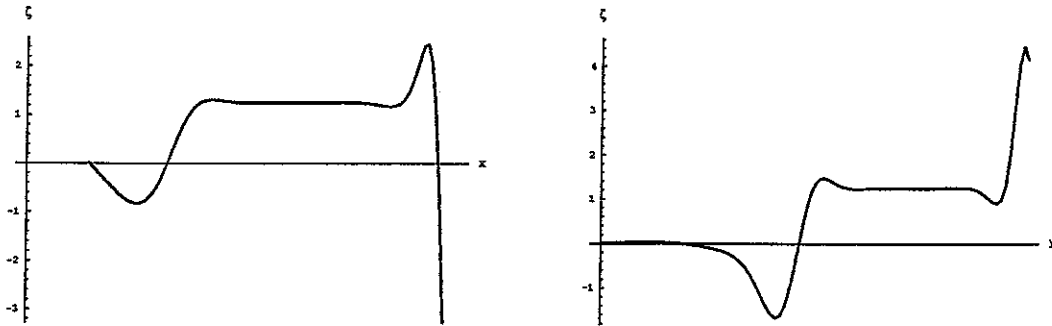


Fig. 6. Vorticity values for  $R = 500$  along  $y = 0.265$  (left) and along  $x = 0.173$  (right).

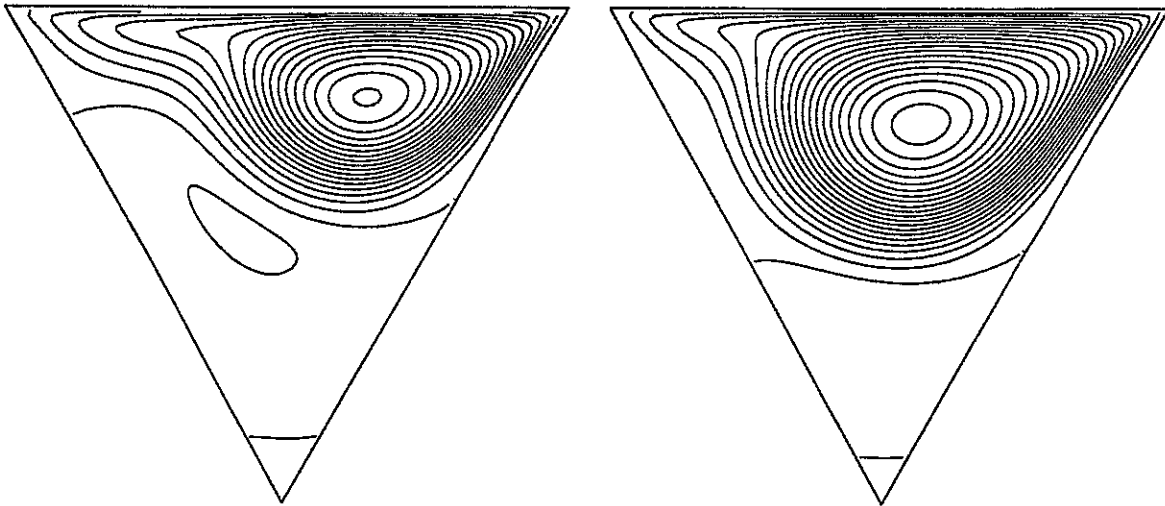


Fig. 7. A spurious solution (left) and the correct solution (right) for  $R = 275$ .

larger as  $R$  is increased (also concluded by Benjamin and Denny [1]). Thus the mean-square law is found to be approximately valid for circular or elliptic boundaries (Ribbens et al. [10]), may be valid for the square cavity if corner eddies are small, but is not valid for the triangular cavity. An interesting experiment for future work would be to test the mean-square law for trapezoidal shaped cavities (of which the square and triangle are limiting cases), with both one side moving and all sides moving.

Another difference between the triangular cavity and the square cavity is in the numerical method. Due to the geometry, especially at the corners, problems arise if standard algorithms are

applied directly. We finally transformed the geometry to an isosceles right triangle and successfully applied a finite difference method, although new formulas had to be derived for the asymmetric stencil in Fig. 3. Care must be taken to use a grid size large enough to be efficiently computationally and small enough such that spurious solutions are not obtained. An example of a spurious solution is shown in Fig. 7.

*Acknowledgements*—The work of Calvin J. Ribbens and Layne T. Watson was supported in part by Department of Energy grant DE-FG05-88ER25068 and Air Force Office of Scientific Research grant 89-0497.

#### REFERENCES

1. R. D. Mills, "On the closed motion of a fluid in a square cavity," *J. Roy Aero. Soc.*, **69**, 116 (1965).
2. F. Pan and A. Acrivos, "Steady flows in rectangular cavities," *J. Fluid Mech.*, **28**, 643 (1967).
3. G. K. Batchelor, "On steady laminar flow with closed streamlines at large Reynolds number," *J. Fluid Mech.*, **1**, 177 (1956).
4. O. R. Burggraf, "Analytical and numerical studies of the structure of steady separate flows," *J. Fluid Mech.*, **24**, 113 (1966).
5. S. Y. Tuann and M. D. Olson, "Review of computing methods for recirculating flow," *J. Comp. Phys.*, **29**, 1 (1978).
6. U. Ghia, K. N. Ghia and C. T. Shin, "High-Re solutions for incompressible flow using the Navier-Stokes equations and a multi-grid method," *J. Comp. Phys.*, **48**, 387 (1982).
7. R. Schreiber and H. B. Keller, "Driven cavity flows by efficient numerical techniques," *J. Comp. Phys.*, **49**, 310 (1983b).
8. A. S. Benjamin and V. E. Denny, "On the convergence of numerical solutions for 2-D flows in a cavity at large Re," *J. Comp. Phys.*, **33**, 340 (1979).
9. R. Schreiber and H. B. Keller, "Spurious solutions in driven cavity calculations," *J. Comp. Phys.*, **49**, 165 (1983a).
10. C. J. Ribbens, C.-Y. Wang, L. T. Watson, and K. A. Alexander, "Vorticity induced by a moving elliptic belt," *Computer Fluids*, **20**, 111 (1991).
11. S. Wolfram, *Mathematica*, Redwood City, California (1988).
12. M. Van Dyke, *Album of Fluid Motion*, Stanford, California (1982).

## Appendix

The  $(i, j)$  entry in the templates below is the coefficient  $\alpha_{ij}$  of  $\Psi(x + ih, y + jh)$  in the finite difference approximation  $\sum_{i,j=-2}^2 \Psi(x + ih, y + jh)$  to a particular partial derivative of  $\Psi$  at  $(x, y)$ .

$$\Psi_x : \frac{1}{2h} \begin{bmatrix} & 0 & 0 \\ 0 & 0 & 0 & 0 \\ 0 & -1 & 0 & 1 & 0 \\ & 0 & 0 & 0 & 0 \\ & & 0 & 0 & \end{bmatrix}, \quad \Psi_y : \frac{1}{2h} \begin{bmatrix} & 0 & 0 \\ 0 & 0 & 1 & 0 \\ 0 & 0 & 0 & 0 & 0 \\ & 0 & -1 & 0 & 0 \\ & & 0 & 0 & \end{bmatrix},$$

$$\Psi_{xx} : \frac{1}{h^2} \begin{bmatrix} & 0 & 0 \\ 0 & 0 & 0 & 0 \\ 0 & 1 & -2 & 1 & 0 \\ & 0 & 0 & 0 & 0 \\ & & 0 & 0 & \end{bmatrix}, \quad \Psi_{xy} : \frac{1}{4h^2} \begin{bmatrix} & 0 & 0 \\ 0 & -1 & 0 & 1 \\ 0 & 0 & 0 & 0 & 0 \\ & 1 & 0 & -1 & 0 \\ & & 0 & 0 & \end{bmatrix},$$

$$\Psi_{yy} : \frac{1}{h^2} \begin{bmatrix} & 0 & 0 \\ 0 & 0 & 1 & 0 \\ 0 & 0 & -2 & 0 & 0 \\ & 0 & 1 & 0 & 0 \\ & & 0 & 0 & \end{bmatrix}, \quad \Psi_{xxx} : \frac{1}{2h^3} \begin{bmatrix} & 0 & 0 \\ 0 & 0 & 0 & 0 \\ -1 & 2 & 0 & -2 & 1 \\ & 0 & 0 & 0 & 0 \\ & & 0 & 0 & \end{bmatrix},$$

$$\Psi_{xxy} : \frac{1}{2h^3} \begin{bmatrix} & 0 & 0 \\ 0 & 1 & -2 & 1 \\ 0 & 0 & 0 & 0 & 0 \\ & -1 & 2 & -1 & 0 \\ & & 0 & 0 & \end{bmatrix}, \quad \Psi_{xyy} : \frac{1}{2h^3} \begin{bmatrix} & 0 & 0 \\ 0 & -1 & 0 & 1 \\ 0 & 2 & 0 & -2 & 0 \\ & -1 & 0 & 1 & 0 \\ & & 0 & 0 & \end{bmatrix},$$

$$\Psi_{yyy} : \frac{1}{2h^3} \begin{bmatrix} & 0 & 1 \\ 0 & 0 & -2 & 0 \\ 0 & 0 & 0 & 0 & 0 \\ & 0 & 2 & 0 & 0 \\ & & -1 & 0 & \end{bmatrix}, \quad \Psi_{xxxx} : \frac{1}{h^4} \begin{bmatrix} & 0 & 0 \\ 0 & 0 & 0 & 0 \\ 1 & -4 & 6 & -4 & 1 \\ & 0 & 0 & 0 & 0 \\ & & 0 & 0 & \end{bmatrix},$$

$$\Psi_{xxyy} : \frac{1}{2h^4} \begin{bmatrix} & 0 & 0 \\ -1 & 3 & -3 & 1 \\ 1 & -4 & 6 & -4 & 1 \\ & 1 & -3 & 3 & -1 \\ & & 0 & 0 & \end{bmatrix}, \quad \Psi_{xyyy} : \frac{1}{h^4} \begin{bmatrix} & 0 & 0 \\ 0 & 1 & -2 & 1 \\ 0 & -2 & 4 & -2 & 0 \\ & 1 & -2 & 1 & 0 \\ & & 0 & 0 & \end{bmatrix},$$

$$\Psi_{xyyy} : \frac{1}{2h^4} \begin{bmatrix} & -1 & 1 \\ 0 & 3 & -4 & 1 \\ 0 & -3 & 6 & -3 & 0 \\ & 1 & -4 & 3 & 0 \\ & & 1 & -1 & \end{bmatrix}, \quad \Psi_{yyyy} : \frac{1}{h^4} \begin{bmatrix} & 0 & 1 \\ 0 & 0 & -4 & 0 \\ 0 & 0 & 6 & 0 & 0 \\ & 0 & -4 & 0 & 0 \\ & & 1 & 0 & \end{bmatrix}.$$